Monthly Notices of the ROYAL ASTRONOMICAL SOCIETY

MNRAS **514,** 3098–3112 (2022) https://doi.org/10.1093/mnras/stac674
Advance Access publication 2022 March 12

Asteroid Lightcurves from the MOA-II Survey: a pilot study

A. J. Cordwell [1]★ N. J. Rattenbury,[1] M. T. Bannister,[2] P. Cowan,[3]
The MOA Collaboration: Fumio Abe,[4] Richard Barry,[5] David P. Bennett,[5] Aparna Bhattacharya,[5,6] Ian A. Bond,[3] Hirosane Fujii,[7] Akihiko Fukui,[8,9] Yoshitaka Itow,[4] Stela Ishitani Silva [5,10] Yuki Hirao,[7] Rintaro Kirikawa,[7] Iona Kondo,[7] Naoki Koshimoto,[5,6] Yutaka Matsubara,[11] Sho Matsumoto,[7] Yasushi Muraki [11] Shota Miyazaki,[7] Arisa Okamura,[7] Clément Ranc,[12] Yuki Satoh,[7] Takahiro Sumi,[7] Daisuke Suzuki,[7] Paul J. Tristram,[13] Taiga Toda,[7] Hibiki Yama[7] and Atsunori Yonehara[14]

[1]*Department of Physics, University of Auckland, Auckland 1010, New Zealand*
[2]*School of Physical and Chemical Sciences - Te Kura Matū, University of Canterbury, Private Bag 5900, Christchurch 9150, New Zealand*
[3]*School of Natural and Computational Sciences, Massey University, Auckland 0856, New Zealand*
[4]*Institute for Space-Earth Environmental Research, Nagoya University, Nagoya 464-8601, Japan*
[5]*Code 667, NASA Goddard Space Flight Center, Greenbelt, MD 20771, USA*
[6]*Department of Astronomy, University of Maryland, College Park, MD 20742, USA*
[7]*Department of Earth and Space Science, Graduate School of Science, Osaka University, Toyonaka, Osaka 560-0043, Japan*
[8]*Instituto de Astrofísica de Canarias, Vía Láctea s/n, E-49306 La Laguna, Tenerife, Spain*
[9]*Department of Earth and Planetary Science, Graduate School of Science, The University of Tokyo, 7-3-1 Hongo, Bunkyo-ku, Tokyo 113-0033, Japan*
[10]*Department of Physics, The Catholic University of America, Washington, DC 20064, USA*
[11]*Department of Physics, University of Warwick, Gibbet Hill Road, Coventry, CV5 8AL, UK*
[12]*Sorbonne Université, CNRS, UMR 7095, Institut d'Astrophysique de Paris, 98 bis bd Arago, F-75014 Paris, France*
[13]*University of Canterbury Mt. John Observatory, PO Box 56, Lake Tekapo 8770, New Zealand*
[14]*Department of Physics, Faculty of Science, Kyoto Sangyo University, 603-8555 Kyoto, Japan*

Accepted 2022 March 9. Received 2022 March 9; in original form 2021 October 13

ABSTRACT

The Microlensing Observations in Astrophysics (MOA-II) survey has performed high cadence, wide field observations of the Galactic Bulge from New Zealand since 2005. The hourly cadence of the survey during eight months of the year, across nearly 50 deg^2 of sky, provides an opportunity to sample asteroid lightcurves in the broad MOA-R filter. We perform photometry of a subset of bright asteroids numbered observed by the survey. We obtain 26 asteroid rotation periods, including for two asteroids where no prior data exist, and present evidence for the possible non-principal axis rotation of (2011) Veteraniya. This archival search could be extended to several thousands of asteroids brighter than 22nd magnitude.

Key words: techniques: photometric – surveys – minor planets, asteroids: general.

1 INTRODUCTION

Only a very small fraction of the million known asteroids have well-measured lightcurves. Asteroid lightcurves can be used to determine the shapes, rotation rates and phase parameters of asteroids. This information is required to correctly interpret results such as estimated diameters from albedoes (Ďurech et al. 2015), complete thermophysical modelling and to plan asteroid space missions (Abell et al. 2015).

The rotation state distribution of asteroids is driven by collisional evolution, tidal interactions, internal structure of asteroids (Pravec & Harris 2000) and the Yarkovsky-O'Keefe-Radzievskii-Paddack (YORP) effect (Pravec et al. 2008). The distribution of periods inferred from light curves features a spin barrier of 2.2 h, below which large 'rubble pile' asteroids breakup (Pravec & Harris 2000). Very few large asteroids that spin faster than this are known (Chang et al. 2019). While periods of tens to hundreds of hours are abundant, surveys from space telescopes suggest an observational bias in existing lightcurve data against asteroids with long rotation periods (Szabó et al. 2016; Pál et al. 2020). Some asteroids are in excited 'tumbling' rotational states (non-principal axis rotation). The cause of this spin state can include spin-up from the YORP effect and sub-catastrophic impacts (Pravec et al. 2005). Developing a larger sample of these objects will help test theoretical mechanisms that modify asteroid rotation (Lee et al. 2020).

Increasing the number of asteroids with known periods will allow for more detailed statistical studies of the asteroid population, studies of the differences between asteroid families, and lead to the identification of rarer types of asteroids. For asteroids with known periods, additional photometry may allow the determination of spin angles and shape models through lightcurve inversion (Kaasalainen

★ E-mail: acor102@aucklanduni.ac.nz, amelia.cordwell@auckland.ac.nz

© 2022 The Author(s).
Published by Oxford University Press on behalf of Royal Astronomical Society. This is an Open Access article distributed under the terms of the Creative Commons Attribution License (http://creativecommons.org/licenses/by/4.0/), which permits unrestricted reuse, distribution, and reproduction in any medium, provided the original work is properly cited.

Downloaded from https://academic.oup.com/mnras/article/514/2/3098/6547784 by guest on 07 November 2023

& Torppa 2001), which requires dense lightcurves from at least three apparitions (Hanuš & Ďurech 2012). These models are necessary for thermophysical modelling (Marciniak et al. 2019) and to further constrain the evolution of asteroid spins.

Many space- and ground-based surveys not deliberately targeting asteroids have been used successfully to determine asteroid rotation rates, such as the K2 mission of the Kepler Space Telescope (Molnár et al. 2018; Marton et al. 2020), TESS (McNeill et al. 2019; Pál et al. 2020), and the Palomar Transient Factory (Waszczak et al. 2015), which reported over 50 000 asteroid lightcurves. These optical surveys have high revisit rates across their footprints.

However, owing to both the sampling and the less in-depth modelling methods used in these surveys, they have a lower success rate in finding period solutions. This has lead to statstical differences in the sets of rotatio periods found by these surveys and by more traditional asteroid period searches (Harris, Pravec & Warner 2012; Warner, Harris & Stephens 2015).

Microlensing surveys typically cover wide areas of the Galactic Bulge and acquire 10–25 epochs of observations per night, over many years. Their large data sets have been used for additional science, such as variable star periods (Li et al. 2017). Gould & Yee (2013) theorized that existing microlensing data could be a good source of asteroid parameters such as rotation rates.

The Microlensing Observations in Astrophysics (MOA) survey is a Japanese, New Zealand and United States collaboration that has been operating the MOA-II survey with a 1.8m telescope in New Zealand since 2006. This paper presents a sample of initial asteroid lightcurve photometry results from the MOA-II database. While the KMTNet microlensing survey has performed asteroid lightcurve photometry during their 'non-bulge season' (Kim et al. 2015), and asteroids were observed in the first iteration of the MOA survey (Bond et al. 2001), this is the first time an existing microlensing dataset has been used for this purpose.

2 THE MOA-II SURVEY

The MOA-II 1.8m telescope at the University of Canterbury's Mt John Observatory in Takapo (Tekapo), New Zealand has performed nightly observations of 22 2.18 deg^2 fields in the Galactic Bulge since 2006, captured on 2k × 4k pixel 10 CCD chips; MOA-cam3 (Sako et al. 2008) with an 0.58″/px plate scale. The primary goal of this survey is to discover exoplanets through microlensing of stars. The survey has a variable cadence, but typically observes each field more than ten times per night. These observations occur from the end of February to the beginning of November while the Galactic Bulge is visible and observe the Large and Small Magellanic clouds at other times.

Galactic Bulge observations are 60 s long, and primarily in the custom MOA-R colour band, which has 90 per cent throughput from 632 to 860 nm (Fig. 1). The fields are observed with a variable cadence, ranging from once per night to thirty times per night, depending on the likelihood of observing microlensing events in that field. Regular V band observations started in 2015 on a far lower cadence: at most once per night. In practice this is even lower, due to poor weather or prioritizing observations of fields with ongoing microlensing events, and we do not make use of them here.

Observations from 2006 to 2010 were recorded on magnetic storage tapes, and have been uploaded to a database. Additionally a record, equivalent to FITS header files but lacking the FITS data, of all observations from 2005 to 2017 was uploaded separately. The deterioration of the physical storage media has caused loss of data; while backups exist, at the time of writing they have not yet been integrated into the database used in this work.

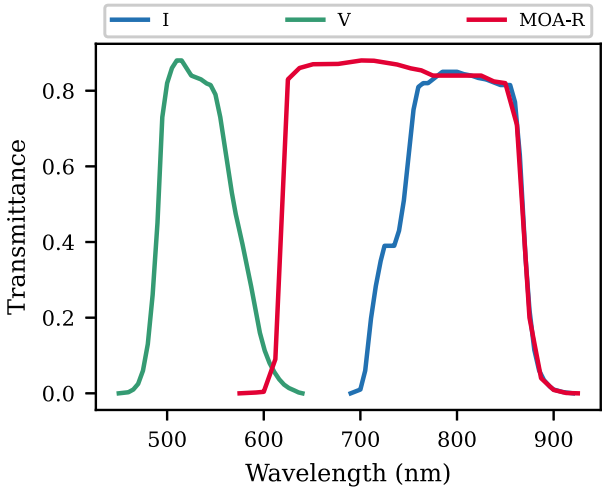

Figure 1. The MOA-II colour filters compare to standard Cousins filters. The MOA-R filter is used for the majority of Galactic Bulge observations and has a similar response to I band filters (Bond et al. 2001). V band observations are occasionally taken by the survey but were not used in this work.

3 METHODOLOGY

3.1 Target selection

A sample of bright asteroids with Minor Planet Center designations numbered between 100 and 4000 were assessed to see if they fell in the MOA-II fields between 2006 and 2010. For each asteroid, nightly ephemerides were obtained from the Minor Planet Center[1] and cross-referenced against the footprints of the 22 MOA-II fields. If the asteroid was near the fields, its ephemerides were calculated during each of the night's MOA-R exposures. If the asteroid is in the field of view of an exposure its pixel, on-sky and orbital position along side the frame name and the Minor Planet Center predicted V magnitude are recorded.

The predicted V magnitude of the object was used to select whether valid photometry of the asteroid would have been recorded by the MOA-II telescope. In I magnitudes, MOA-II standard R frames have a saturation magnitude of ≈13 and a limiting magnitude of ≈19 (21 under exceptional seeing; median site seeing is above 1.5″). Under the assumption of asteroid colour indices being $V - I \approx 1$ the asteroid V magnitude limits were set between 14.5 and 19.

3.2 Photometry

Photometry was attempted for asteroids numbered that met the magnitude requirements in more than 30 MOA-II observation frames. All data were obtained from the MOA-II database and re-reduced in full; no use was made of the standard MOA-II differencing image analysis Bond et al. (2001).

The frames were calibrated with dark and flat frames, then cropped to 512 x 512 pixel sub frames (a small border was included to

[1] https://minorplanetcenter.net/iau/MPEph/MPEph.html

Downloaded from https://academic.oup.com/mnras/article/514/2/3098/6547784 by guest on 07 November 2023

account for asteroids near the edge of the sub frame). Owing to the crowded nature of the MOA-II fields, difference imaging analysis was used to provide photometry. In difference imaging analysis individual observation images are compared to high quality reference images of the same field (Alard & Lupton 1998). A kernel is computed to transform the reference image to match the observation image to account for changes in seeing and background sky brightness. The transformed reference image is subtracted from the observation to create a difference image. The difference image will contain only the changes in brightness, such as due to a new object entering the field or a stellar magnification event (Bond et al. 2001). Difference imaging and photometry was performed using the `pyDIA` difference imaging software Albrow (2017), with photometry computed on the difference image using point spread function fitting.

While difference imaging analysis can remove the need for full photometric calibration in finding periodicity for stationary objects, as asteroids will move across the different chips and fields of the telescope, a calibration procedure to standard magnitudes is required.

We used a set of standard MOA-II reference images for each of the fields, with baseline photometry and transformation coefficients from MOA-Red magnitudes to Cousins I magnitudes. These coefficients were generated where the MOA-II reference fields overlap with the OGLE fields. Missing coefficients are replaced with those for the nearest field on the same CCD chip. The asteroid's colour index is not taken into account in this transformation.

The baseline MOA-II photometry was completed using different software, as such the computed pyDIA instrumental magnitudes had to be transformed first into the MOA-II reference instrumental magnitudes, before the transformation to Cousins I magnitudes could take place. This was achieved using 25 randomly selected comparison stars on each cropped sub-frame. To avoid variable stars affecting the calibration, the photometric flux of each comparison star on the difference image is required to be smaller than the uncertainty on the difference frame and reference frame added in quadrature. If more than seven of the comparison stars are rejected then the photometry from this image is rejected.

3.3 Lightcurve analysis

The lightcurve of an asteroid in a visible colour band can be described as

$$V = H + \delta + 5log_{10}(r\Delta) + 2.5log_{10}(\phi(\alpha)) \quad (1)$$

Where V is the apparent visual magnitude, H is the absolute magnitude, r is the Sun-asteroid distance in A.U., Δ is the Earth-asteroid distance in A.U., δ describes the rotational and shape variation. $\phi(\alpha)$ is the phase function, where α represents the phase angle, the angle between the Earth, the asteroid and the Sun. While δ is most accurately determined by computing the light reflected from a complex rotating shape model, the shapes of many asteroids are approximated well by a Jacobi ellipsoid. On time scales much shorter than the orbital period of the asteroid, the variation can be approximated by a sine wave with a frequency twice the actual rotation frequency.

We follow a similar method as in Waszczak et al. (2015) to simultaneously fit rotation periods and phase parameters, by performing a 2D linear least squares grid search. We model the rotational component of the lightcurve as a second-order Fourier series and model the phase function using the Lumme-Bowell model Bowell et al. (1989) defined as

$$\phi = (1 - G)\phi_1 + G\phi_2 \text{ where} \quad (2)$$

$$\phi_1 = \exp(-3.33\tan^{0.63}[\alpha/2]), \text{ and} \quad (3)$$

$$\phi_2 = \exp(-1.87\tan^{1.22}[\alpha/2]). \quad (4)$$

Lightcurves are first pre-processed by subtracting the distance contribution. Large outliers due to photometric error are removed by computing a linear fit across the full curve and removing any data points more than 3 std from the linear fit. This process is repeated until no data points are removed in a single pass, or fewer than 20 data points remain which causes the analysis to cease.

For each pair of possible phase parameters, G, and rotation frequencies, F, the reduced I magnitude y_i' ise calculated as

$$y_i' = y_i - 2.5log_{10}(\phi[G, \alpha_i]), \quad (5)$$

where α_i is the asteroid's solar phase angle during the exposure and y_i is the distance-corrected observation. A linear least squares fit is then carried out using the design matrix, A, below, where t_i is the lighttime corrected midtime of the exposure y_i minus the midtime of the first photometric data point and

$$A = \begin{bmatrix} 1 \\ \sin(2\pi F t_i) \\ \cos(2\pi F t_i) \\ \sin(4\pi F t_i) \\ \cos(4\pi F t_i) \end{bmatrix}. \quad (6)$$

Phase parameter (G) values are searched from -0.3 to 0.7 with a step size of 0.005 [following Waszczak et al. (2015)]. The range of frequency values are chosen based on ΔT, the time between the first and last observations of the asteroid. Frequencies tested range from $F_{\max} = 1/(1.8/24)\text{JD}^{-1}$ to $F_{\min} = \delta F = \max(1/4\Delta T, 1/(4 \cdot 30 \cdot 6)\text{JD}^{-1})$ where δF is also the frequency step size. The minimum bound on δF is included primarily to constrain computation time. These steps follow Waszczak et al. (2015).

The initial best-fitting frequency and phase parameters are selected based on the lowest χ^2 value. However as asteroid lightcurves are typically expected to be double-peaked around the asteroid's physical rotation frequency, we test the folded lightcurve for the presence of multiple peaks. If the lightcurve only has a single peak, then the solution at half that frequency is checked. For that solution if the $\Delta\chi^2$ between that and $\chi^2_{\min}$ is less than the inverse χ^2 distribution for 7 degrees of freedom at 97 per cent confidence, it is accepted as the best solution.

We estimated the 1σ uncertainty limits in F and G by considering the frequency or phase parameter range that had a χ^2 value lower than $\chi^2_{\min} + \Delta\chi^2$ where $\Delta\chi^2$ is inverse χ^2 distribution for 68 per cent with $N_{obs} - 7$ degrees of freedom. Subsequently, the 1σ uncertainty in period is taken by finding the periods at the edges of the confidence interval and averaging their differences from the best-fitting period. The uncertainty in the absolute magnitude is the relevant parameter in the covariance matrix from the linear least squares fitting added in quadrature to the uncertainty of the H value based on the uncertainty limits in G.

The lightcurves were checked for any secondary frequency signals by performing an additional set of frequency fitting on the residuals. The best-fitting model was subtracted from each original lightcurve, and a first order Fourier series was fit for the same set of frequencies as in the main analysis. The χ^2 goodness of fit was calculated for each frequency.

Downloaded from https://academic.oup.com/mnras/article/514/2/3098/6547784 by guest on 07 November 2023

Table 1. The performance of the photometry pipeline as applied to asteroids in this study. This was significantly affected by missing data in the MOA-II database.

	Count	Percent
Total possible observations	23 916	100%
with complete source and calibration images	10 010	42%
and without saturated pixels on the object	9897	41%
and where photometric calibration completed	6272	26%
and where no software errors occurred.	5957	5%

4 RESULTS

4.1 Observed asteroid sample

Asteroids numbered from 100 and 3999 were checked for their coincidences with observations in the MOA-II database from 2006 to 2010. Of these 1045 of those coincided with observations at least once with 407 coinciding more than 30 times. Main belt asteroids had the highest likelihood of coinciding with observations, 28 per cent of which had at least once coincidence with MOA observations whereas only 19 per cent of Trojan asteroids and 5 per cent of Near Earth Objects coincided, respectively.

Owing to the variable cadence of the different MOA-II fields, some asteroids were observed upwards of 40 times in a single night, whereas others had on the order of five observations in a single night and observations spread over multiple weeks. Owing to weather conditions at Mount John, gaps of days between observing an asteroid are common. Multi-opposition sequences exist: 68 asteroids were observed at least twice with a gap of over 6 months between successive observations.

Records of observations from the MOA-II telescope without the image data were available up until 2017. To see how the additional seven years of survey data would improve the sampling of observations, we considered the subset of 500 asteroids numbered between 2000 and 2499, 17 per cent were within MOA-II observations more than 30 times between 2005 and 2010 whereas 35 per cent were between 2005 and 2017.

4.2 Photometric performance

Photometry was attempted for the 125 asteroids numbered between 2000 and 3000 that were within more than 30 MOA observations. More than 30 photometric datapoints were only able to be extracted for 60 of those. Table 1 shows the final outcome of each processing attempt. The most significant loss of data was due to observations that were made my MOA but did not have restored.fits data. A significant number of possible observations were rejected due to the photometric 'goodness' cut-off. Replacing the missing observations in the database would increase the percentage of MOA observations providing a photometric data point from 25 to 60 per cent.

The calculated photometric error was far less than the actual photometric scatter in the derived lightcurves. Partial lightcurves for some asteroids at high cadences do show that the formal photometric error is a good estimate of the error. This suggests that the majority of this error is due to the photometric calibration process as the asteroid is observed on different fields or on different CCD chips, which are subject to different calibration.

As either creating more accurate calibration coefficients or defining a MOA-R stellar catalogue is out of scope for proving that the database could be used for asteroid work, we instead artificially inflate the error bars. To calculate this we first took a sample of asteroids that had a quality period solution in the Lightcurve Database (LCDB) Warner, Harris & Pravec (2009) that matched our calculated best-fitting period within 2 per cent. (For this case, we defined quality to have an LCDB rating U = 2 or above.) The residual of each data point from the best-fitting period model was calculated and divided by the formal photometric error. This gives a normal distribution of the residuals in units of the formal error. The standard deviation of this was found to be 8.345, and as such we inflated all photometric error bars by that value.

4.3 Period solutions

Table 2 shows period solutions that are considered to be unambiguous, and Table 3 shows period solutions that the MOA-II data does not completely unambiguously constrain. An example of the output for the code used to determine these classifications can be seen in Fig. 2 which shows the output for Asteroid 2043. Figures for the rest of the asteroids in Tables 2 and 3 are in the appendix.

The minimum lightcurve amplitude for all the unambiguous periods was 0.14 mag, and for less unambiguous solutions 0.10 mag. This limit is tied directly to the current photometric uncertainties. Some asteroids had solutions rejected automatically that matched with previously reported periods. These were typically in low amplitude lightcurves and suggest asteroids that could be well fit with corrected photometric calibration.

4.4 Evidence for potential non-principle axis rotation of asteroid 2011

Asteroid 2011 (Fig. 4) was well sampled in the MOA-II observations with sets of dense nightly observations within one month, followed by smaller set of observations 5 months later as it crossed back through the MOA-II fields.

The shape of the frequency χ^2 field (Fig. 3d) suggested an additional frequency at 8.2 h. The standard analysis method was re-completed with a restriction on all periods being below 12 h. This showed a rotation period of 8.234 h. The folded lightcurve at this period clearly follows the model line across all parts of the rotational phase except it had a gap between two groupings of observations. Finally a single order Fourier series was fit to the residuals of the lightcurve subtracted by the initial long period model in Fig. 3(e). This shows that the 8.234-h period is separate to the longer period signal. It is therefore possible that this asteroid is undergoing non-principal axis rotation.

Identification of the length of the longer rotation period will require further analysis such as a two dimensional Fourier series search (Pravec et al. 2005), and the possible inclusion of additional sets of observation to prevent issues rotational period aliasing. However the data and analysis presented here do show evidence for possible non-principle axis rotation occurring.

Hasegawa et al. (2014) found that Asteroid 2011 had a rotation period of 8.209 h, however the length of time they observed the asteroid for was too short to have observed the rotational variation seen here.

4.5 Phase parameters and absolute magnitudes

As most of the dense sets of observations were from within a single opposition, few lightcurves were able to be used to accurately constrain a phase parameter. The best attempts in constraining a phase parameter are shown in Table 4. The results show a difference

Downloaded from https://academic.oup.com/mnras/article/514/2/3098/6547784 by guest on 07 November 2023

Table 2. Asteroids where MOA-II data was able to provide an unambiguous constraint on their rotation period. Graphs of these lightcurves can be found in Figs A1–A3.

Asteroid ID	Rotation period (h)	Amplitude (Mag)	Literature Period (h)	LCDB Quality	Reference
2010	4.1060 ± 0.0041	0.3			
2011	$8.23427 \pm 8.2e-09^{*\#}$	0.5	8.2096 ± 0.0003	3-	Hasegawa et al. (2014)
2022	14.143 ± 0.014	0.5	14.1385 ± 0.0031	3-	Haro-Corzo et al. (2018)
2043	$7.74776 \pm 7.7e-08$	0.5	7.7475 ± 0.0005	3-	Lang (2015)
2133	$4.06314 \pm 4.1e-09^{*}$	0.5	4.05616 ± 0.00005	3-	Pravec et al. (2021)
2310	15.990 ± 0.016	0.5	16.169 ± 0.003	3-	Odden et al. (2016)
2511	$4.14167 \pm 4.1e-09^{*}$	0.7	4.1403 ± 0.0004	3	Waszczak et al. (2015)
2565	2.0570 ± 0.0021	0.5	2.1498 ± 0.0004	2	Waszczak et al. (2015)
2617	11.776 ± 0.012	0.5	11.7729 ± 0.0006	3	Behrend (2021)
2630	19.407 ± 0.019	0.7	19.4283	2	Ďurech et al. (2016)
2663	3.964 ± 0.004	0.8	3.957489	2	Ďurech, Hanuš & Alí-Lagoa (2018)
2681	4.2230 ± 0.0042	0.3	4.22235 ± 0.00005	3-	Behrend (2021)
2756	27.085 ± 0.027	0.4			
2947	$10.95751 \pm 1.1e-07^{\#}$	0.7	10.430 ± 0.001	3-	Aznar Macias (2016)

Note. * indicates that the double period solution was required to be forced, and # indicates that the final reduced χ^2 value was above 3. Amplitudes are measured as half of peak to trough distance from the model lightcurve. Quality measures are taken from the Lightcurve Database Warner et al. (2009), where a 2 indicates some period ambiguity and a 3 represents an unambiguous solution. Where multiple measurements of a lightcurve is given in the literature only either the highest quality or lowest uncertainty value included in the Lightcurve Database is used.

Table 3. Asteroids where the MOA-II derived periods do not provide a completely unambiguous constraint. Graphs of these lightcurves can be found in Figs B1–B3.

Asteroid ID	Rotation period (h)	Amplitude (Mag)	Literature Period (h)	LCDB Quality	Reference
2162	$5.71091 \pm 5.7e-09$	0.2	8.1048 ± 0.0005	2	Pravec et al. (2021)
2224	$62.44374 \pm 6.2e-05$	0.7	27.0 ± 0.4	3-	Slivan et al. (2008)
2263	$35.52841 \pm 3.6e-06$	0.4	41.7 ± 0.1	2-	Warner (2011) @
2280	$14.83625 \pm 1.5e-06^{\#}$	1	21.45 ± 0.01	3-	Linville et al. (2017)
2403	$153.07908 \pm 1.5e-05^{\#}$	1			
2554	$345.03499 \pm 3.5e-05$	$> 0.5^{\$}$	273 ± 1	2	Skiff (2013) @
2558	4.7860 ± 0.0048	0.7	4.784 ± 0.002	3-	Ditteon et al. (2018)
2592	$25.39706 \pm 2.5e-07^{\$}$	0.6	49.9871	2	Ďurech et al. (2018)
2620	$4.35594 \pm 4.4e-09$	0.7	3.3918 ± 0.0005 h	2	Waszczak et al. (2015)
2659	$6.12411 \pm 6.1e-09$	0.5	6.132 ± 0.002	3	Wisniewski et al. (1997)
2762	$5.30930 \pm 5.3e-09^{*\#}$	0.6	5.295 ± 0.001	3-	Menzies (2013)
2930	$15.32948 \pm 1.5e-07$	0.9			
2988	$29.35459 \pm 2.9e-07$	0.8	29.494 ± 0.001	3	Gross (2003)

Note. * indicates that the double period solution was manually forced, and # indicates that the final reduced χ^2 value was above 3. Amplitudes are measured as half of peak to trough distance from the model lightcurve. $ indicates that the standard analysis gave an incorrect amplitude due to the coverage across the rotational phase of the lightcurve. Quality measures are taken from the Lightcurve Database Warner et al. (2009), where a 2 indicates some period ambiguity and a 3 represents an unambiguous solution. Where multiple measurements of a lightcurve is given in the literature only either the highest quality or lowest uncertainty value included in the Lightcurve Database is used. References with an @ next to them indicate the original source did not consider their rotation period constraint to be unambiguous.

between absolute magnitude estimates from MOA-II data and the Minor Planet Center, due to the different colour filters in use.

5 DISCUSSION

Of the 125 asteroids numbered between 2000 and 3000 that were observed more than 30 times by the MOA-II survey between 2005 and 2010, 26 were able to have rotation periods determined using the MOA-II data. The resultant asteroid rotation periods are plotted against the broader populatioon of asteroids (Fig. 4). 14 of these rotation periods were considered well constrained, and of the 12 that had existing periods in the literature all matched previous periods within 5 per cent although only half matched within formal uncertainty limits.[2]

Only four of the eleven asteroids with with ambiguous period derivations from MOA-II data matched literature reported periods within 5 per cent, although two of the literature periods were themselves ambiguous. Only one asteroid (2558) matched within

[2]For asteroids where the existing literature did not include a period uncertainty, we estimate their uncertainty as being the same as the MOA uncertainty for that asteroid's period.

Downloaded from https://academic.oup.com/mnras/article/514/2/3098/6547784 by guest on 07 November 2023

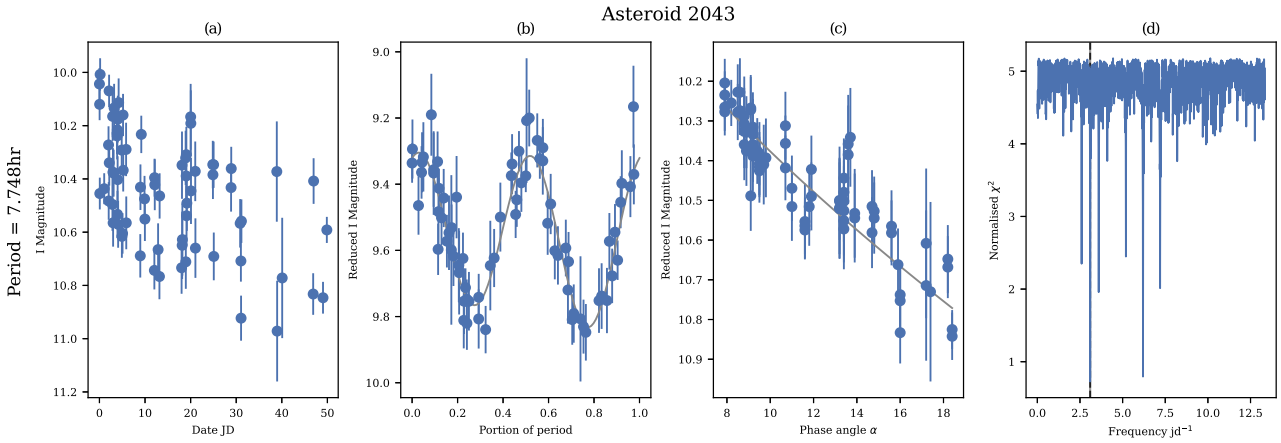

Figure 2. Lightcurve and analysis results output for Asteroid 2043 Ortutay. (a) shows the observed lightcurve with the distance correction applied. The zero date was set at the time of the first observation. Further figures may have observations in additional colours based on temporal grouping. (b) shows the folded lightcurve at the best-fitting period, with distance and phase effects removed. The calculated lightcurve model is shown in grey. (c) shows the observed phase relationship with the rotational model subtracted. The fitted phase model is shown in grey. (d) shows the periodogram at the best-fitted phase parameter. The black dotted line indicates the best-fitted frequency and the grey lines around it indicate the 1σ uncertainty frequency bounds.

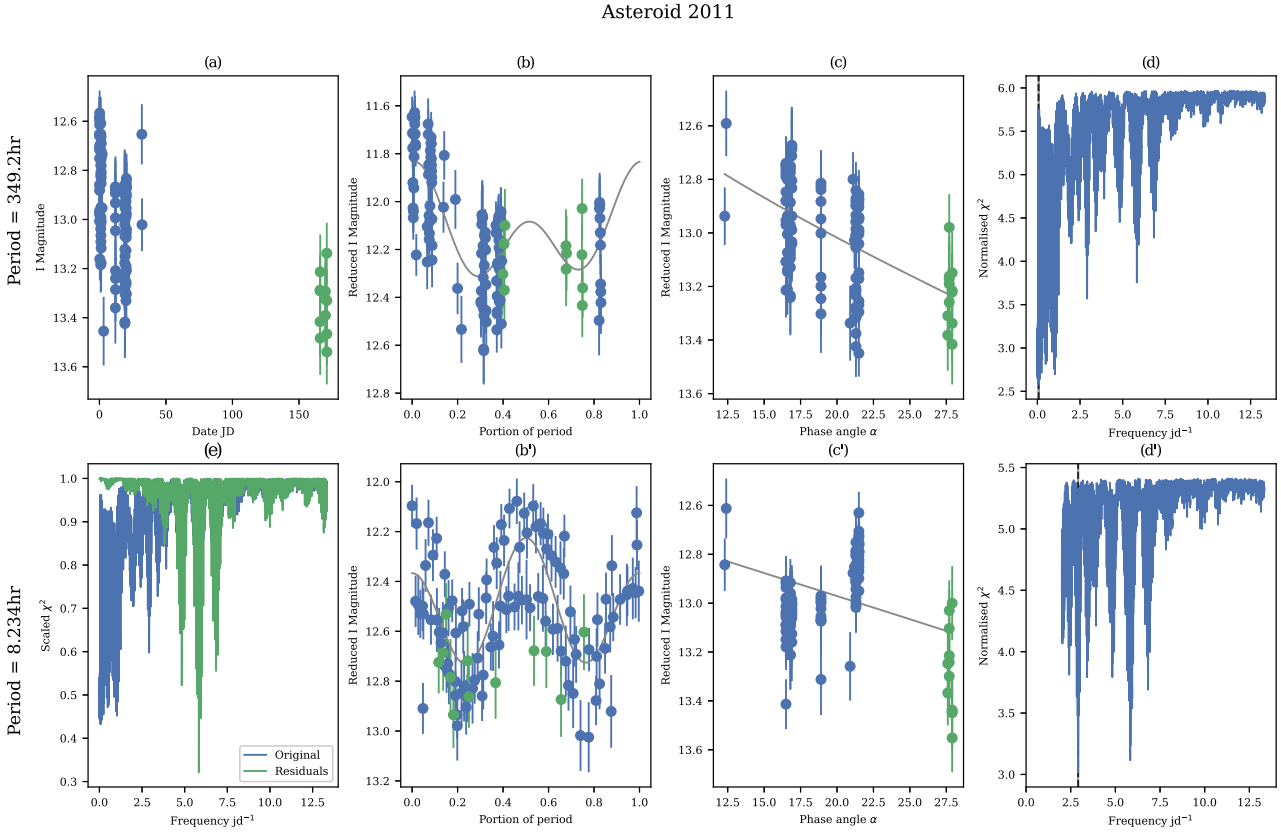

Figure 3. Lightcurves and Periodograms for Asteroid 2011. Plots (a)–(d) are cover the same analysis as in Fig. 2 but for 2011, Plots (b')–(d') repeat that with a restriction that only considers periods shorter than 12 h. (e) Compares the shape of the initial χ^2 fit, to the χ^2 generated by performing a first order Fourier fit on the residuals of the data from the model presented in (b). The initial fit for this asteroid suggested an unphysical light curve and the residual periodogram (bottom figure) suggested that there was at least one other physical period at 8.2 h. The shape of this lightcurve seems more likely, however there is a offset between different nights observations of this light curve, potentially due to NPA rotation.

Downloaded from https://academic.oup.com/mnras/article/514/2/3098/6547784 by guest on 07 November 2023

Table 4. H-G estimates for asteroids from MOA-II data ordered by minimum uncertainty in G. The Minor Planet Center (MPO H) H estimates have been retrieved from the JPL Small Body Browser Jet Propulsion Laboratory (2019). PS1 (Pan-STARRS) G estimates are from Vereš et al. (2015), and are included where available, G estimates marked with a ⋆ are instead from the Palomar Transient Factory Waszczak et al. (2015), which did not include uncertainty estimates. The difference between the Minor Planet Center H and the MOA-II H can be interpreted as a V-MOARed colour index, however as they use a different phase parameter they are not directly comparable.

Asteroid ID	H	± H	G	± G	# Points	MPO H	PS1 G	Note
2721	11.16	0.01	−0.005	0.0125	45	12.3	0.450 ± 0.122	
2043	9.55	0.05	−0.045	0.0725	73	10.8	−0.023 ± 0.139	
2520	10.50	0.10	−0.08	0.1375	206	11.8		
2947	12.09	0.17	0.34	0.245	93	12.8		Reduced $\chi^2 > 3$
2280	12.59	0.25	0.4	0.28	38	13.3	−0.026 ± 0.098	
2360	11.80	0.20	0.11	0.285	60	12.9	0.309 ± 0.164	
2511	12.06	0.28	0.54	0.2975	81	12.7	0.275⋆	

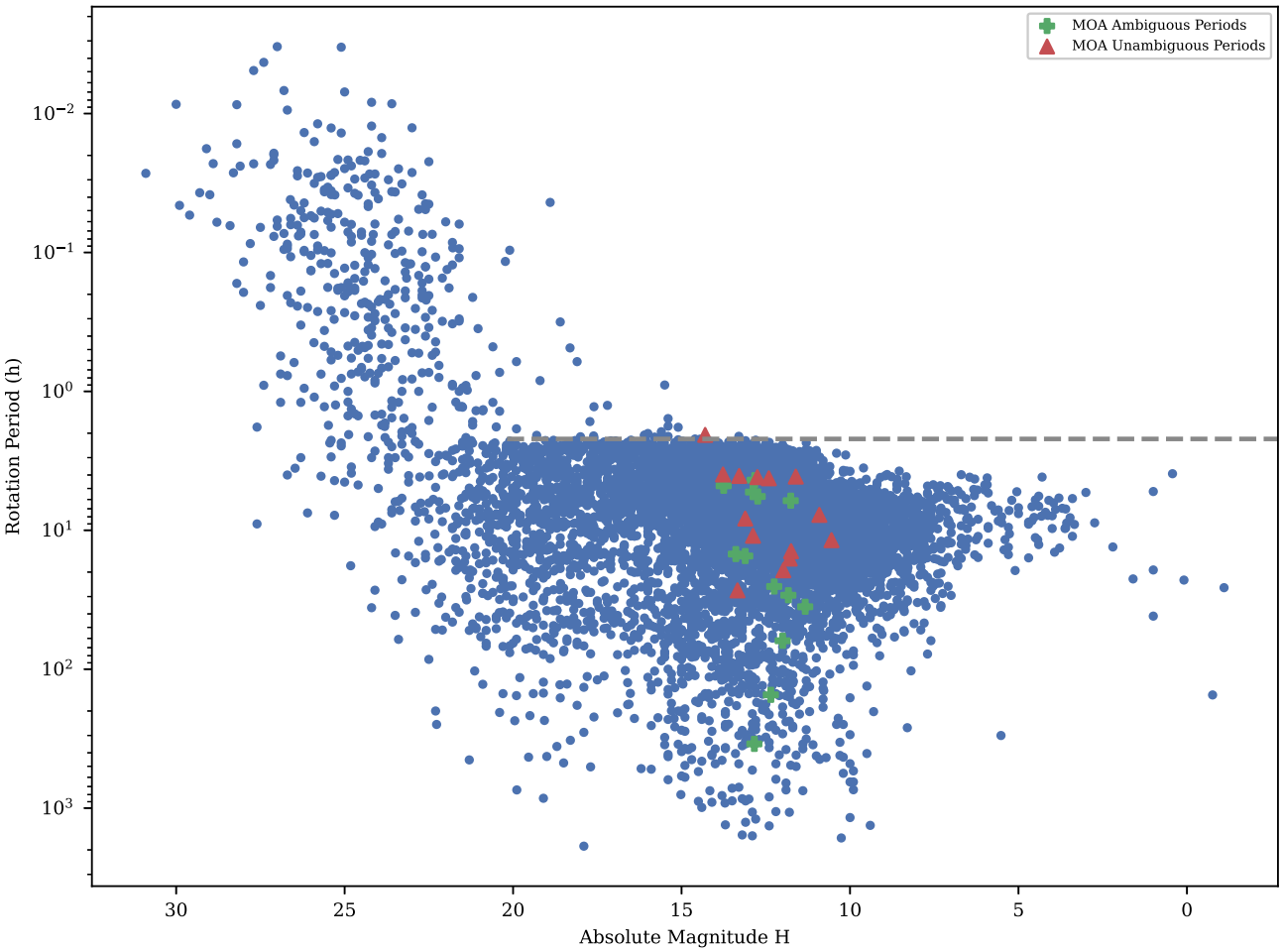

Figure 4. The distribution of asteroid rotation periods derived in this work compared to the periods in the F_D-BASIC file of the Lightcurve Database (Warner et al. 2009). Absolute magnitude values for asteroids with a MOA period have been retrieved from the JPL Small Body Browser (Jet Propulsion Laboratory 2019). The distribution in absolute magnitudes follow from the distribution in absolute magnitudes for asteroids numbered between 2000 and 3000. As the ambiguous MOA-II period solutions tend to be larger than the unambiguous periods there is likely some bias against the identification of longer periods.

the formal error. These identifications were at least successful at identifying the order of magnitude of the period, which may be useful for identifying asteroids with long rotation periods for further study. We also consider the uncertainty estimates on the ambiguous periods to be unreliable. Especially with long baselines, neighbouring frequencies may have the effect of shifting the folded lightcurve out of phase with itself, but other nearby frequencies may have similar goodness of fit. Fig. 4 shows that the MOA-II data is biased against

Downloaded from https://academic.oup.com/mnras/article/514/2/3098/6547784 by guest on 07 November 2023

properly constraining long (>12 h) periods compared to shorter periods. Unambiguously constraining these periods would require further coverage of their rotation from targeted follow up. This is a known bias in the literature from ground-based surveys, especially when applied to more detailed models, (Marciniak et al. 2019) and needs to be accounted for in population studies (Warner & Harris 2011).

The distribution of asteroid absolute magnitudes follows from the selection of the sample of asteroids numbered between 2000 and 3000. Based on the limiting and saturation magnitudes of the MOA-II data, the spread of absolute magnitudes from a larger sample of asteroids that pass through these fields would be much wider.

Fewer than half of the 125 asteroids that photometry was attempted for ended up having enough observations for period analysis. For these asteroids the MOA-II data had a 25 per cent unambiguous period identification rate. This compares favorably to other similar studies such as the Palomar Transient Factory (PTF) (Waszczak et al. 2015), which had a success rate of 17 per cent for lightcurves with >20 photometric data points. However only 24 per cent of possible asteroid observations gave usable photometry. The majority of this loss is due to missing data. As work has now been completed to restore missing data from a second copy of the database, further work beyond this proof-of-concept study would expect denser sampling in the available photometry.

Attempts to use this data set to constrain phase parameters were limited as for most asteroids the phase curve was typically not well sampled in the 2006–2010 period, and there was significant scatter even after rotational effects were accounted for.

Due to the error bar inflation we were unable to constrain the rotation periods of asteroids with amplitudes below 0.1 mag. Significant losses in photometric accuracy compared to the possible photometric quality of the MOA-II dataset were introduced due to the lack of accurate photometric calibration causing a large number of asteroids with low lightcurve amplitudes to be rejected. Developing a better procedure for MOA-II photometric calibration would increase the performance of this system and allow period identification for asteroids with lower amplitude lightcurves, as well as increase the ability for these lightcurves to be used detailed shape modelling processes.

In addition all, but one object with a solution has an amplitude < 0.3 magnitudes. This limit is possibly related to the choice of a second order Fourier model, as below this limit the higher order shape harmonics can dominate the lightcurve (Harris et al. 2014). While this is acceptable for a pilot program, more detailed modelling should be used in future with this dataset. This, as well as more human review of results, will be required to identify the lightcurves of rarer types of asteroids.

The MOA-II database could be used in future to determine rotation periods for a far larger number of asteroids. As the photometry pipeline works on a per asteroid basis, this could also be applied to specific asteroids or groups of asteroids of interest.

6 CONCLUSION

In this work, we derived rotation periods for 26 asteroids based on historical lightcurve observations in the MOA-II database. We confirmed many of these against measured periods in the literature, presented four previously unmeasured rotation periods and provided evidence for the possible nonprincipal-axis rotation of asteroid 2011.

In future, the MOA-II database could be used to determine rotation periods for a far larger number of asteroids, although this is hampered by the lack of precision photometric calibration currently available.

ACKNOWLEDGEMENTS

The Nectar Research Cloud was used in completion of this research. The MOA project is supported by JSPS KAKENHI Grant Number JSPS24253004, JSPS26247023, JSPS23340064, JSPS15H00781, JP16H06287, 17H02871, and 19KK0082. The work by CR was supported by the ANR project COLD-WORLDS of the Agence Nationale de la Recherche with the reference ANR-18-CE31-0002. MTB appreciates support by the Rutherford Discovery Fellowships from New Zealand Government funding, administered by the Royal Society Te Apārangi. We thank the reviewer Brian D. Warner for his insightful comments.

DATA AVAILABILITY

The photometric data underlying this article will be made available on the CDS webservice.

REFERENCES

Abell P. A., Barbee B. W., Chodas P. W., Kawaguchi J., Landis R. R., Mazanek D. D., Michel P., 2015, Human Exploration of Near-Earth Asteroids. Univ. Arizona Press, Tuscon, AZ, p. 855
Alard C., Lupton R. H., 1998, ApJ, 503, 325
Albrow M. D., 2017, Michaeldalbrow/pydia: Initial release on github. Zenodo. Available at: https://doi.org/10.5281/zenodo.268049
Aznar Macias A., 2016, Minor Planet Bulletin, 43, 350
Behrend R., 2021, Courbes de rotation d'astéroïdes et de comètes. Available at: http://obswww.unige.ch/~behrend/page_cou.html
Bond I. A. et al., 2001, MNRAS, 327, 868
Bowell E., Hapke B., Domingue D., Lumme K., Peltoniemi J., Harris A. W., 1989, in Binzel R. P., Gehrels T., Matthews M. S., eds, Asteroids II. Univ. Arizona Press, Tuscon, AZ, p. 524
Chang C.-K. et al., 2019, ApJS, 241, 6
Ditteon R., Black S., Masner Z., Osborne J., Trent L., 2018, Minor Planet Bulletin, 45, 338
Ďurech J., Carry B., Delbo M., Kaasalainen M., Viikinkoski M., 2015, in Patrick M., Francesca E. D., William F. B., eds, Asteroids IV. Univ. Arizona Press, Tuscon, AZ, p. 183
Ďurech J., Hanuš J., Oszkiewicz D., Vančo R., 2016, A&A, 587, A48
Ďurech J., Hanuš J., Alí-Lagoa V., 2018, A&A, 617, A57
Gould A., Yee J. C., 2013, ApJ, 767, 42
Gross J., 2003, Minor Planet Bulletin, 30, 44
Hanuš J., Ďurech J., 2012, Planet Space Sci, 73, 75
Haro-Corzo S. A. R. et al., 2018, Minor Planet Bulletin, 45, 233
Harris A. W., Pravec P., Warner B. D., 2012, Icarus, 221, 226
Harris A. W. et al., 2014, Icarus, 235, 55
Hasegawa S. et al., 2014, PASJ, 66, 54
Jet Propulsion Laboratory, 2019, JPL Small-body Database Browser. Available at: https://ssd.jpl.nasa.gov/sbdb.cgi
Kaasalainen M., Torppa J., 2001, Icarus, 153, 24
Kim M.-J., Moon H.-K., Choi Y.-J., Yim H.-S., Bae Y.-H., Roh D.-G., Park J. T., Moon B., 2015, Proc. IAU Vol. 10, DEEP-South: Preliminary Photometric Results from the KMTNet-CTIO. Cambridge Univ. Press, Cambridge, p. 313
Lang K., 2015, Minor Planet Bulletin, 42, 136
Lee H. J. et al., 2020, A&A, 635, A137
Li M. C. A. et al., 2017, MNRAS, 470, 539
Linville D., Jiang H., Michalik D., Wilson S., Ditteon R., 2017, Minor Planet Bulletin, 44, 173
McNeill A., Mommert M., Trilling D. E., Llama J., Skiff B., 2019, ApJS, 245, 29
Marciniak A. et al., 2019, A&A, 625, A139
Marton G. et al., 2020, Icarus, 345, 113721
Menzies K., 2013, Minor Planet.info: CALL: Search Results. Available at: http://www.minorplanet.info/call.html

Downloaded from https://academic.oup.com/mnras/article/514/2/3098/6547784 by guest on 07 November 2023

Molnár L. et al., 2018, ApJS, 234, 37
Odden C. E. et al., 2016, Minor Planet Bulletin, 43, 99
Pál A. et al., 2020, ApJS, 247, 26
Pravec P., Harris A. W., 2000, Icarus, 148, 12
Pravec P. et al., 2005, Icarus, 173, 108
Pravec P. et al., 2008, Icarus, 197, 497
Pravec P., Scheirich P., Kusnirak P., Hornoch K., Galád A., Velen M., 2021, Ondrejov Asteroid Photometry Project. Available at: http://www.asu.cas.cz/~ppravec/neo.html
Sako T. et al., 2008, Exp. Astron., 22, 51
Skiff B. A., 2013, Minor Planet.info: CALL: Search Results. Available at: http://www.minorplanet.info/call.html
Slivan S. M. et al., 2008, Icarus, 195, 226
Szabó R. et al., 2016, A&A, 596, A40
Vereš P. et al., 2015, Icarus, 261, 34
Warner B. D., 2011, Minor Planet Bulletin, 38, 89
Warner B. D., Harris A. W., 2011, Icarus, 216, 610
Warner B. D., Harris A. W., Pravec P., 2009, Icarus, 202, 134
Warner B. D., Harris A. W., Stephens R. D., 2015, Review of Rotation Statistics with and without the Results from Wide-field Surveys. Conference poster, AAS, DPS meeting #47, id.307.02
Waszczak A. et al., 2015, AJ, 150, 75
Wisniewski W. Z., Michałowski T. M., Harris A. W., McMillan R. S., 1997, Icarus, 126, 395

Downloaded from https://academic.oup.com/mnras/article/514/2/3098/6547784 by guest on 07 November 2023

APPENDIX A: UNAMBIGUOUSLY CONSTRAINED ASTEROID LIGHTCURVES

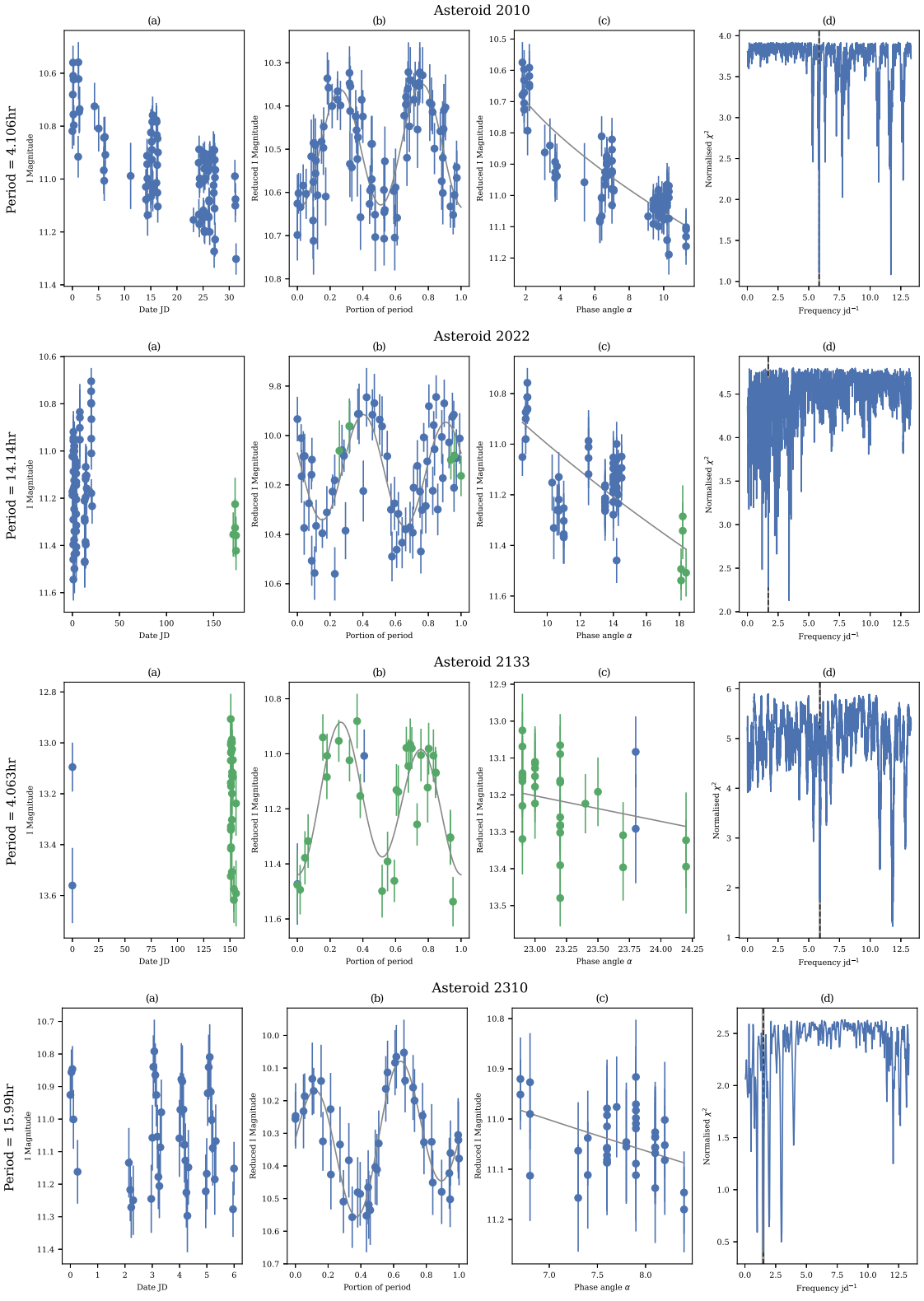

Figure A1. Analysis output for asteroids 2010, 2022, 2133, and 2310. (Double period solution enforced for 2133).

Downloaded from https://academic.oup.com/mnras/article/514/2/3098/6547784 by guest on 07 November 2023

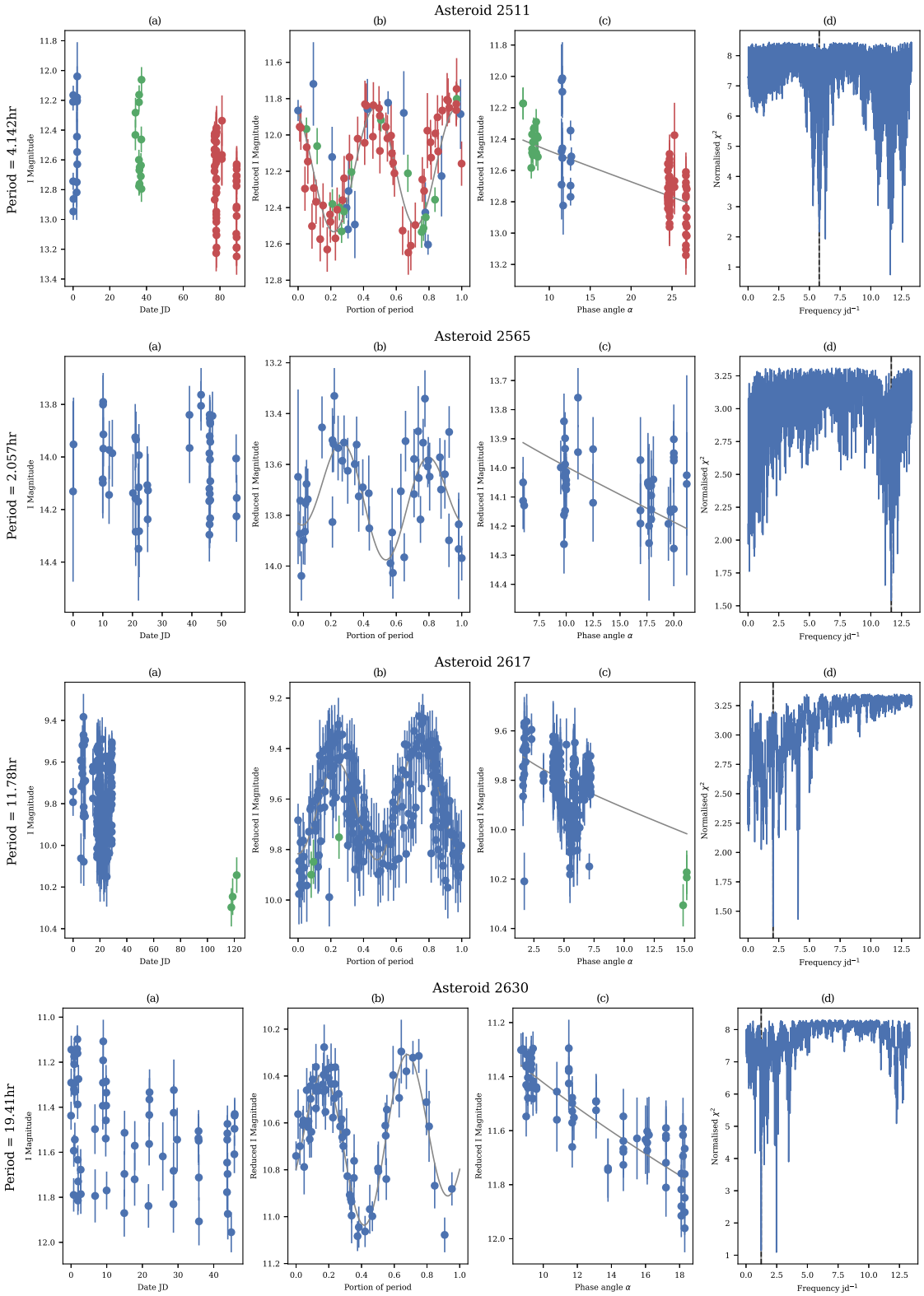

Figure A2. Analysis output for asteroids 2511, 2565, 2617, and 2630. (Double period solution enforced for 2511).

Downloaded from https://academic.oup.com/mnras/article/514/2/3098/6547784 by guest on 07 November 2023

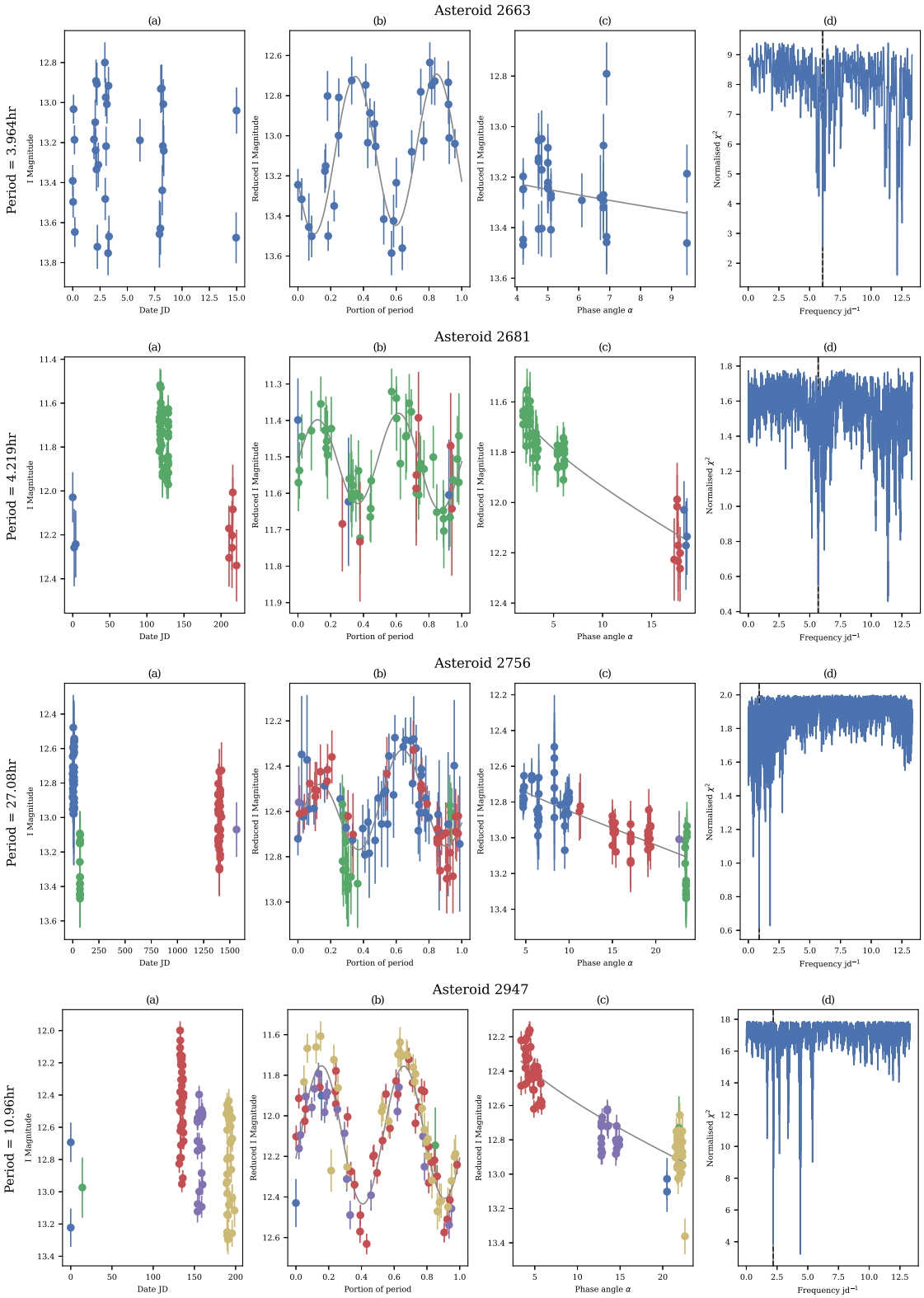

Figure A3. Analysis output for asteroids 2663, 2681, 2756, and 2947.

Downloaded from https://academic.oup.com/mnras/article/514/2/3098/6547784 by guest on 07 November 2023

APPENDIX B: AMBIGUOUSLY CONSTRAINED ASTEROID LIGHTCURVES

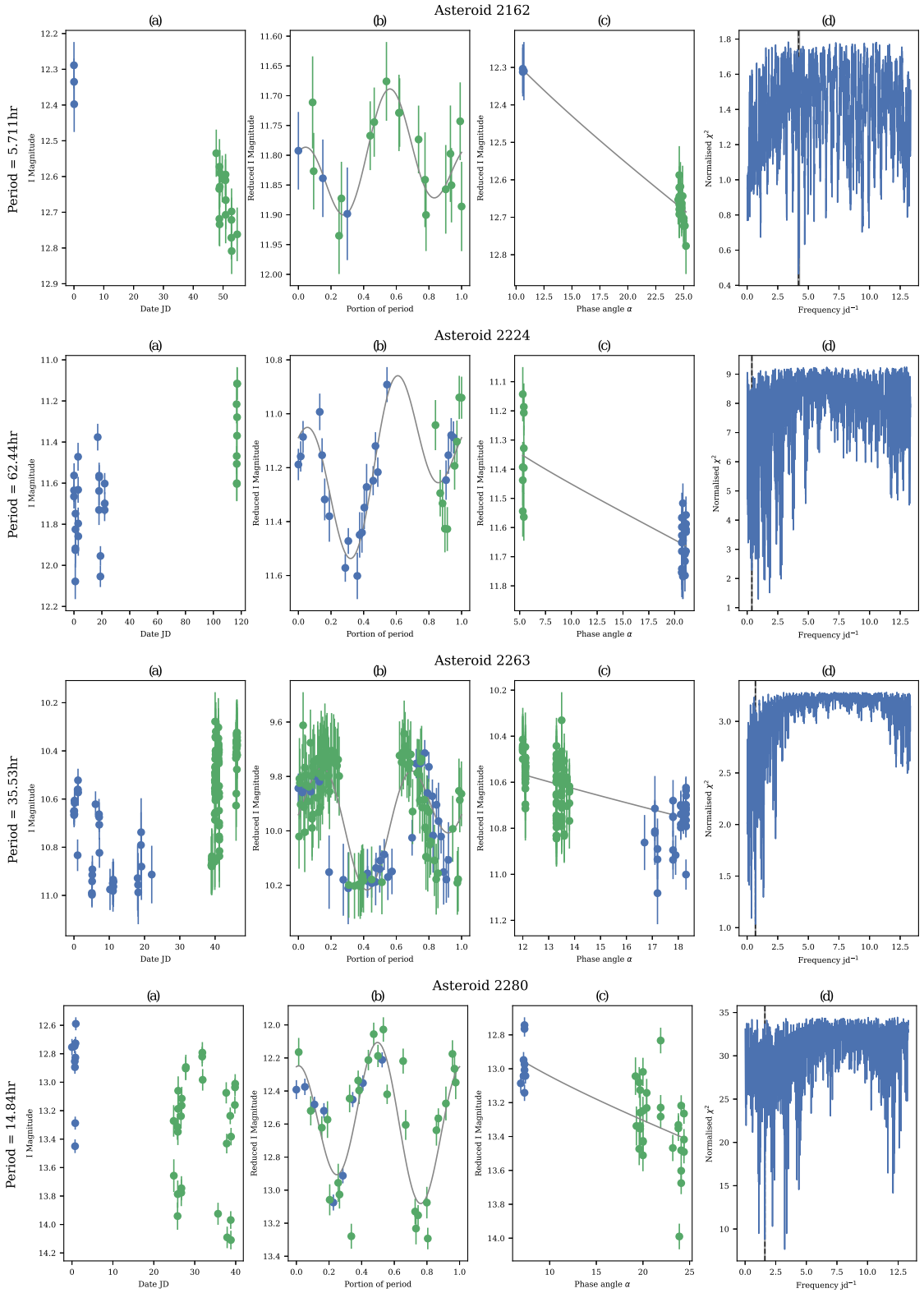

Figure B1. Analysis output for asteroids 2162, 2224, 2263, and 2280.

Downloaded from https://academic.oup.com/mnras/article/514/2/3098/6547784 by guest on 07 November 2023

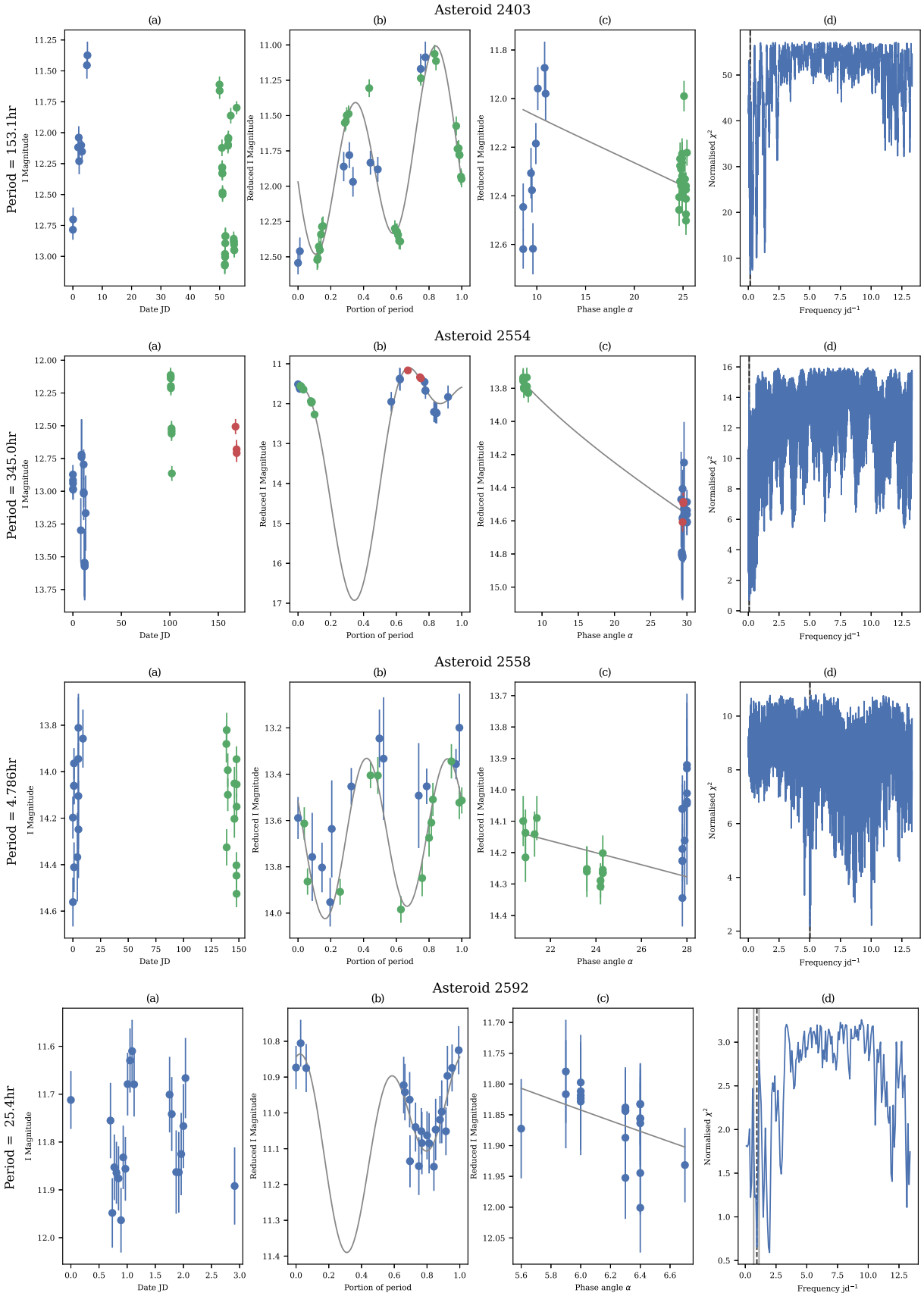

Figure B2. Analysis output for asteroids 2403, 2554, 2558, and 2592. Asteroid 2403 had analysis repeated for the second epoch of data only, from which the same period was calculated.

Downloaded from https://academic.oup.com/mnras/article/514/2/3098/6547784 by guest on 07 November 2023

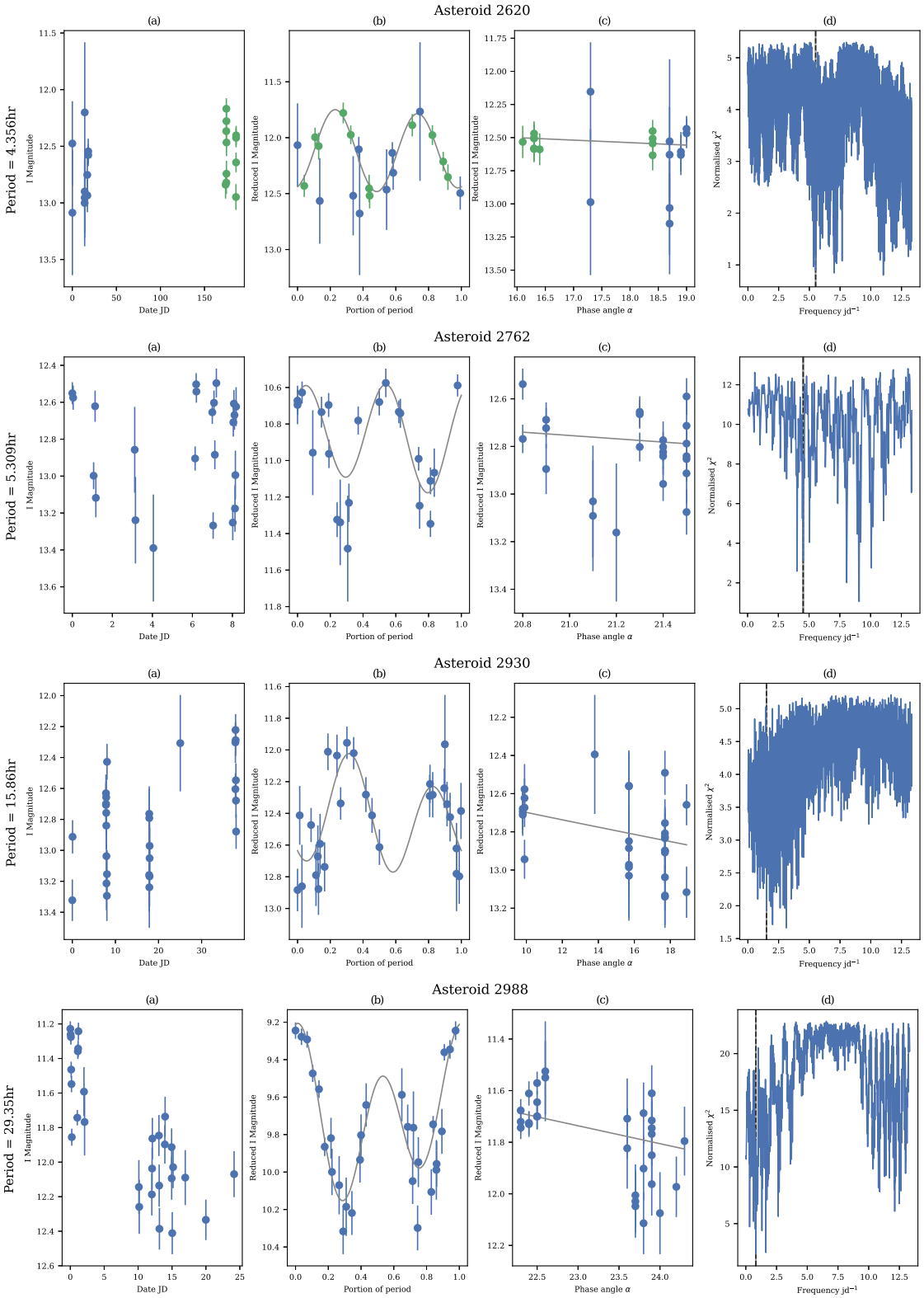

Figure B3. Analysis output for asteroids 2620, 2762, 2930, and 2988.

This paper has been typeset from a TEX/LATEX file prepared by the author.

Downloaded from https://academic.oup.com/mnras/article/514/2/3098/6547784 by guest on 07 November 2023